Confined Vortex Shedding Past a Square Cylinder with a Planar Jet*

Do-Hyeong KIM**, Kyung-Soo YANG**
and Jun-Seok EOM**

In this investigation, confined vortex shedding past a square cylinder with a planar jet is numerically studied. Flow and scalar-transport simulations are presented for various cases including both laminar and turbulent flow situations. It is shown that the ratio of jet velocity to uniform inlet velocity significantly affects the overall flow structures and thus scalar transport downstream of the cylinder. Especially, when the ratio is large enough, the jet penetrates the main vortices shed from the cylinder, resulting in significant changes in the flow and scalar fields. In the case of laminar flow, regions of intense scalar are formed along the streamlines from the jet exit, and the oscillation of the force on the cylinder eventually disappears as the jet velocity is close to the inlet velocity. Large Eddy Simulation of turbulent flow also reveals complex flow structures and intense mixing depending on the velocity ratio; regions of intense scalar coincide with those of high turbulence intensity. The results obtained exhibit fuel-air mixing characteristics observed in a planar combustor where the square cylinder plays the role of a flame-holder.

Key Words: Turbulence, Large Eddy Simulation, Vortex Shedding, Square Cylinder

1. Introduction

Kármán vortex shedding past a cylindrical obstacle has been a lasting research subject for many investigators not only for academic reasons but also for a wide variety of engineering applications using the flow phenomenon. One of the main features of this flow configuration is a periodic force loading in streamwise and vertical directions due to the pressure difference on the cylinder surface caused by the periodic vortex shedding. If the loading frequency is close to the natural frequency of the cylindrical structure, resonance may severely damage the structure.

One can find numerous references in the literature regarding the vortex shedding and its control. Most of them are experimental or numerical studies on 'external' vortex shedding, i.e. the obstacle is placed in an infinite flow domain. Both circular[1]-[4] and square cylinders[5],[6] have been considered. However, studies on the 'confined' vortex shedding[7],[8] in internal flows such as channel flows are relatively rare. In this flow configuration, the vortex shedding is considerably affected by the presence of the wall boundaries; in particular, numerical difficulties in flow computation have been reported in association with this type of vortex shedding[7].

In this study, numerical simulation of confined vortex shedding past a square rib is performed both in laminar and in turbulent flow regimes. Especially, a jet injected from the rib into the flow field is also included, and a parametric study is carried out in each regime with various values of Injection Ratio (*IR*, the ratio of jet velocity to mean inlet velocity) in order to see how the jet can influence the pattern of vortex shedding and subsequent force loading on the rib.

The physical configuration (Fig. 1) considered in this study can be regarded as a model geometry for a planar combustor in which a two-dimensional (2D) fuel jet is injected in the combustion chamber and the rib plays the role of a flame-holder[9]. In this regard, additional simulations of scalar transport are also performed to clarify fuel-air mixing characteristics in the situation of nonpremixed combustion in a planar

* Received 30th September, 2002 (No. 02-5155)
** Department of Mechanical Engineering, Inha University, Incheon, 402-020, Republic of Korea. E-mail: ksyang@inha.ac.kr

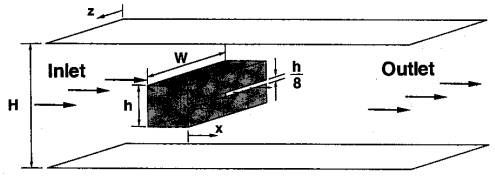

Fig. 1 Physical configuration

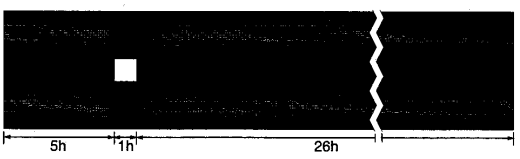

Fig. 2 Grid system

combustor. Physical dimensions of our computational domain are exactly matched to those of the experimental setup of Koutmos et al.[9]

2. Formulation and Numerical Method

All variables are normalized by the mean inlet velocity (U_m) and the obstacle height (h). The code uses a nonuniform Cartesian staggered grid in a finite-volume approach. In the case of laminar vortex shedding, the 2D incompressible equations of continuity, momentum balance, and scalar transport are used as governing equations;

$$\frac{\partial u}{\partial x}+\frac{\partial v}{\partial y}=0 \tag{1}$$

$$\frac{\partial u}{\partial t}+u\frac{\partial u}{\partial x}+v\frac{\partial u}{\partial y}=-\frac{\partial p}{\partial x}+\frac{1}{Re}\left(\frac{\partial^2 u}{\partial x^2}+\frac{\partial^2 u}{\partial y^2}\right) \tag{2}$$

$$\frac{\partial v}{\partial t}+u\frac{\partial v}{\partial x}+v\frac{\partial v}{\partial y}=-\frac{\partial p}{\partial y}+\frac{1}{Re}\left(\frac{\partial^2 v}{\partial x^2}+\frac{\partial^2 v}{\partial y^2}\right) \tag{3}$$

$$\frac{\partial \phi}{\partial t}+u\frac{\partial \phi}{\partial x}+v\frac{\partial \phi}{\partial y}=\alpha_m\left(\frac{\partial^2 \phi}{\partial x^2}+\frac{\partial^2 \phi}{\partial y^2}\right) \tag{4}$$

where u, v are velocities in x(streamwise) and y (normal) directions, respectively; p, Re, ϕ and α_m denote pressure, Reynolds number, mass fraction of fuel, and molecular diffusivity, respectively.

Large Eddy Simulation(LES) is employed for turbulent vortex shedding. After filtering the full incompressible equations of continuity, momentum balance, and scalar transport using a volume-average box filter, we obtain the following governing equations for LES;

$$\frac{\partial \bar{u}_j}{\partial x_j}=0 \tag{5}$$

$$\frac{\partial \bar{u}_i}{\partial t}+\frac{\partial(\bar{u}_i\bar{u}_j)}{\partial x_j}=-\frac{\partial \bar{p}}{\partial x_i}-\frac{\partial}{\partial x_j}\tau_{ij}+\frac{1}{Re}\frac{\partial^2 \bar{u}_i}{\partial x_j \partial x_j} \tag{6}$$

$$\frac{\partial \bar{\phi}}{\partial t}+\frac{\partial}{\partial x_j}(\bar{u}_j\bar{\phi})=\frac{\partial}{\partial x_j}\left(\alpha_m\frac{\partial \bar{\phi}}{\partial x_j}-q_j\right) \tag{7}$$

where u_1, u_2, u_3 (or u, v, w) are velocities in x_1 (streamwise), x_2 (normal), x_3 (spanwise) directions (or x, y, z), respectively, and $q_j=\overline{u_j\phi}-\bar{u}_j\bar{\phi}$; the overline represents filtered quantities. Ethane ($\alpha_m=0.148\times10^{-4}\ m^2/s$) of which density is close to that of air, is selected as fuel in both cases.

The equations must be closed by modeling the subgrid-scale stresses (τ_{ij}) and scalar transport flux (q_j) terms. See Yang & Ferziger[10] and Akselvoll & Moin[11] for details on the subgrid-scale modelling. A dynamic procedure to determine model coefficients (C_s) is employed in both τ_{ij} and q_j modelling. Figure 2 shows the grid system used in this work; the rib is placed at the center in y.

To advance the solution in time, a fractional step method[12] is employed. The time-advancement of the momentum equations is hybrid; the convective terms are explicitly advanced by a third-order Runge-Kutta scheme and the viscous terms implicitly by Crank-Nicolson method. For flow field, a second-order accurate central differencing is utilized for spatial discretization except for convection terms in 2D laminar computation where LUDS(Linear Upwind Difference Scheme) is employed. For scalar field, QUICK(Quadratic Upstream Interpolation for Convective Kinematics) upwind scheme is used for accuracy in convective terms. To accelerate computation time, a multigrid method is implemented in solving the Poisson equation obtained by fractional step method. The code is fully vectorized; it runs at a typical speed of 1.5GFLOPS on NEC SX-4. See Yang & Ferziger[10] for detailed description of the numerical method used in the code.

3. Results and Discussion

3.1 Laminar vortex shedding and scalar transport

A 2D laminar computation is carried out at $Re=200$ in order to study characteristics of the laminar confined vortex shedding with a jet. A convective boundary condition[13] is imposed at the exit for both velocity and scalar fields. On the solid boundaries, the no-slip boundary condition is used for u_i while a Neumann condition is imposed for ϕ.

The vertical width of the jet is set as $h/8$ and the blockage ratio (H/h) is fixed as 6. A grid-refinement study is carried out to determine a proper numerical resolution. A grid system of 288×144 in the streamwise and the normal directions, respectively, is selected for the main simulation; no significant improvements are obtained with more finer grids.

3.1.1 Code verification To verify our code, computation is performed for a benchmark case of

$H/h=6$ and $IR=0$ for which numerous numerical and experimental data are available in the literature. Figure 3 shows comparison of the present Strouhal number (St) with those of other authors for the range of $Re=200-600$. Two types of inlet velocity profiles are considered, namely parabolic and uniform profiles, because the actual profile in the experiment[14] is not exactly known. The present results properly bound the experimental values, and are in an excellent agreement with the numerical ones of Davis et al.[14] and Cho & Kang[15].

3.1.2 Rear jet In Fig. 4, are shown time-averaged velocity and scalar fields for the rear jets of $IR=0.235$, $IR=0.53$, and $IR=1.54$. In the cases of small IR, the jet does not have enough momentum to affect the main vortices generated by flow separation at the front corners of the square rib (Figs. 4(a) and 4(b)).

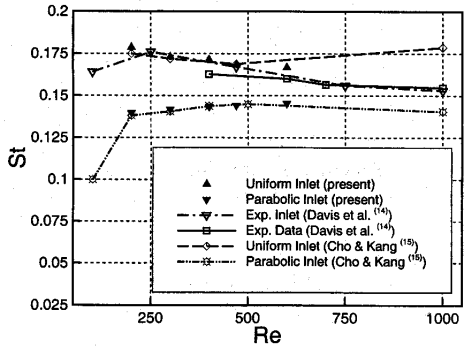

Fig. 3 Comparison of Strouhal number

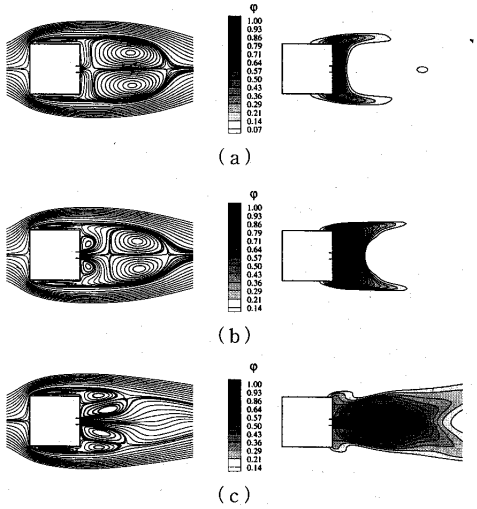

Fig. 4 Time-averaged streamlines and ϕ contours for rear jet, $Re=200$; (a) $IR=0.235$, (b) $IR=0.53$, (c) $IR=1.54$

Consequently, high concentration of fuel is noticed between the rear face of the cylinder and the vortices. In the case of high IR, however, the jet has enough momentum to penetrate further downstream of the cylinder. The main vortices completely disappear while new vortices are formed near the rear corners. Furthermore, the pair of counter-rotating vortices induced by the jet elongates in the streamwise direction. In all the three cases, the regions of high ϕ are formed along the streamlines of the jet, indicating that convection is the main mechanism for the scalar transport than diffusion for this particular fuel.

Figure 5 shows the time histories of the drag coefficient $\left(C_D=Drag\Big/\frac{1}{2}\rho U_m^2 A\right.$, where ρ is the density of the fluid, and A is the frontal area of the cylinder$\left.\right)$ computed using pressure difference and friction, and the total drag coefficient ($C_{D,jet}$) which further includes the jet momentum in the drag calculation. It turns out that the viscous drag is negligible compared with the form drag in all cases. The jet is suddenly injected into the fully develped flow field of $IR=0$ at $t=194$ where t is the nondimensionalized

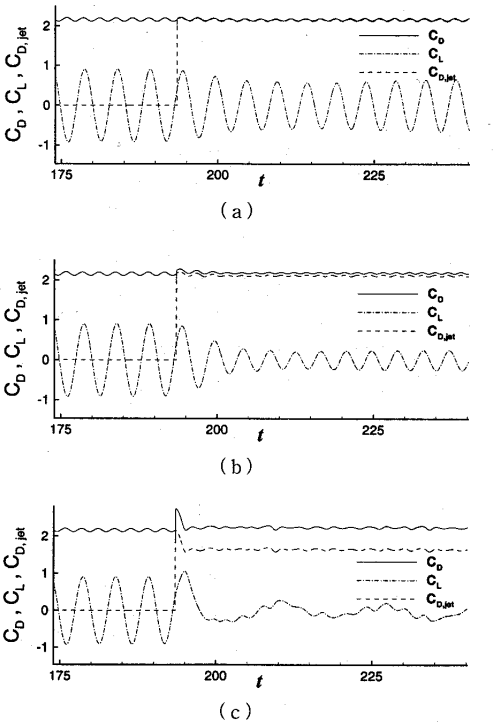

Fig. 5 Drag and Lift coefficients for rear jet, $Re=200$; (a) $IR=0.235$, (b) $IR=0.53$, (c) $IR=1.54$. The jet is suddenly injected at $t=194$.

Table 1 Mean and RMS fluctuation values of C_D, C_L and $C_{D,jet}$

		No jet	IR(Front jet)			IR(Rear jet)		
			0.235	0.53	1.54	0.235	0.53	1.54
mean	C_D	2.16	2.17	2.14	1.24	2.17	2.19	2.24
	$C_{D,jet}$	2.16	2.18	2.20	1.83	2.16	2.12	1.65
RMS fluc.	C_D	3.11×10^{-2}	3.85×10^{-2}	4.81×10^{-2}	0.110	2.24×10^{-2}	1.39×10^{-2}	2.38×10^{-2}
	C_L	0.639	0.748	0.871	0.612	0.438	0.169	0.140
	$C_{D,jet}$	3.11×10^{-2}	3.85×10^{-2}	4.81×10^{-2}	0.110	2.24×10^{-2}	1.39×10^{-2}	2.38×10^{-2}

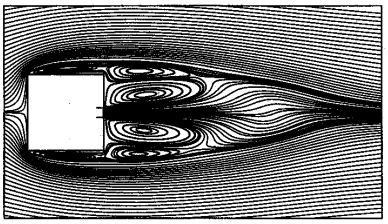

Fig. 6 Time-averaged streamlines at $Re=200$, $IR=1.20$

time. The fluctuation of the lift coefficient $\left(C_L=Lift\Big/\frac{1}{2}\rho U_m^2 A\right)$ is significantly reduced as IR increases. This is due to the fact that the jet pushes the vortices shed from the cylinder further downstream (Figs. 4(a) and 4(b)) and eventually weakens them (Fig. 4(c)) so that the shed vortices less affect the vertical force loading on the cylinder. However, the drag caused by the pressure difference between the front and the rear faces is less reduced or even slightly increased by the presence of the jet. Nevertheless, $C_{D,jet}$ is considerably reduced due to the jet momentum. Mean and root-mean-squared(RMS) fluctuation values of C_D, $C_{D,jet}$ and C_L are summarized in Table 1.

The structural change of the main vortices (Fig. 4(c)) is observed over $IR=1.1$. Turbulent flows also reveal averaged velocity fields similar to Fig. 4(c). Figure 6 shows time-averaged streamlines of present computation at $IR=1.20$. Comparing the numerical result with the corresponding experimental one of Koutmos et al.[9] (Fig. 4 in their article), one can notice a striking resemblance between the two.

In the range of $IR<1.1$, fluctuations of C_D and C_L are suppressed as IR increases, while vortex structures downstream of the cylinder remain topologically unchanged. See Figs. 4(a), 4(b), Figs. 5(a), 5(b), and Table 1. However, in the range of $IR>1.1$, a drastic change of the vortex structures occurs (Fig. 4(c) and Fig. 6), and the trend of fluctuations of C_D and C_L is reversed with increasing IR (Fig. 5(c) and Table 1). From this, one can conjecture that there must be an optimal value of IR at which each fluctuation is minimal. To obtain this value, more simulations have been performed; the result is presented in

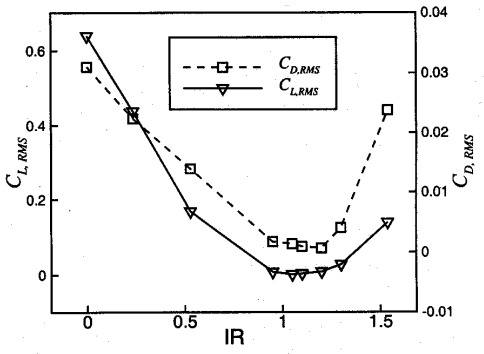

Fig. 7 RMS fluctuations of C_D and C_L for various IR, $Re=200$

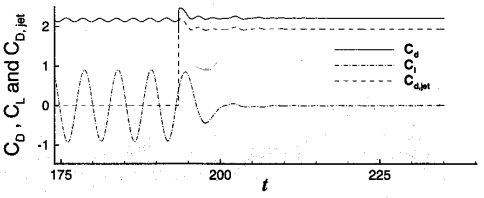

Fig. 8 Drag and lift coefficients for a rear jet at $Re=200$, $IR=1.05$. The jet is suddenly injected at $t=194$.

Fig. 7. RMS fluctuation of C_D has the minimum value at $IR=1.2$ while the minimum RMS fluctuation of C_L is identified near $IR=1.05$. It should be noted that the periodic lift force almost vanishes near $IR=1.05$. Figure 8 shows the time histories of C_D and C_L at this particular IR which confirms our observation. Figure 9 presents a sequence of instantaneous pressure contours around the square cylinder at $IR=1.05$. The main vortices due to the leading-edge separation are pushed further downstream by the jet; the cylinder becomes less affected by the vortices. It can be noticed that the contours are almost stationary in the vicinity of the cylinder except in the rear region; this explains the significant reduction of fluctuations in lift and drag forces.

For the confined vortex shedding past a square cylinder without a jet ($IR=0$), the size of the recirculation bubble behind the cylinder is mainly determined by the inlet velocity. In the range of $IR<1.1$, however, the jet reduces the bubble size as IR increases (Figs. 10(a), 10(b), and 10(c)); the bub-

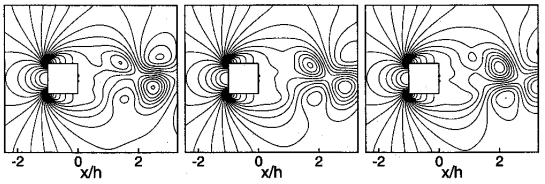

(a) t=216.620 (b) t=217.113 (c) t=217.605

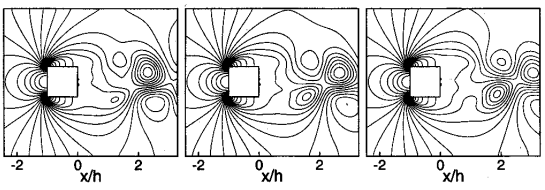

(d) t=218.098 (e) t=218.590 (f) t=219.083

Fig. 9 Pressure contours at Re=200, IR=1.05

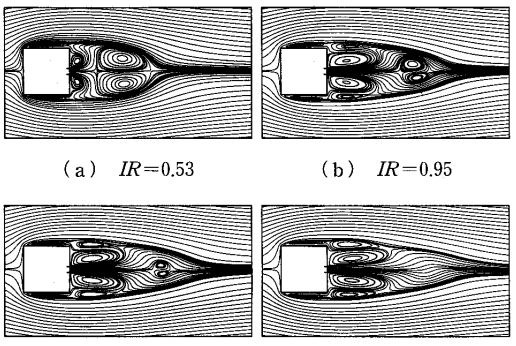

(a) IR=0.53 (b) IR=0.95

(c) IR=1.05 (d) IR=1.20

Fig. 10 Time-averaged streamlines for various IR, Re=200

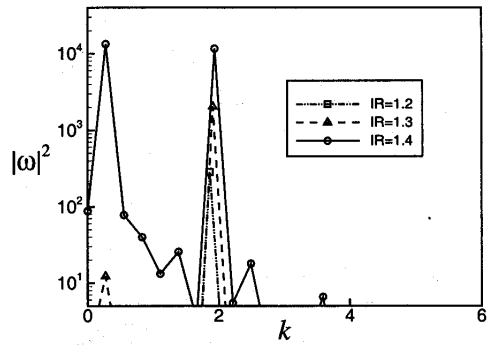

Fig. 11 Energy of Fourier modes where ω is Fourier coefficient, Re=200.

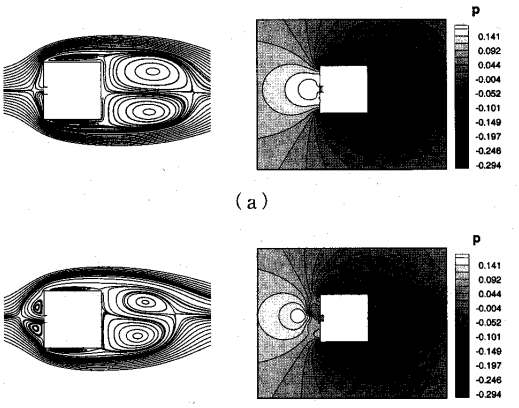

(a)

(b)

Fig. 12 Time-averaged streamlines and pressure contours for front jet, Re=200; (a) IR=0.53 (b) IR=1.54

ble completely disappears at IR=1.2 (Fig. 10(d)).

Figure 11 reveals two dominant peaks in the energy spectrum obtained by Fourier transform of the time-dependent C_L for IR=1.4, namely at k=0.28, and 1.96 where k is the nondimensionalized wavenumber. Figure 11 also shows the cases for IR=1.2 and 1.3. It is noticed that the mode at k=0.28 grows significantly as IR increases, while the mode at k=1.96 is dominant in all the cases. For high IR, the vortices induced by the jet are shed, increasing the energy of the mode at k=0.28.

3.1.3 Front jet Since the flow slows down as it approaches the cylinder, the pressure on the front face is very high. One can thus anticipate a significant drag reduction by pushing the high-pressure region upstream by a front jet, even though it may not be an economical way of reducing drag. Figures 12 and 13 are corresponding to Figs. 4 and 5, respectively. The lift fluctuation initially gets bigger as IR increases, because the flow rate accordingly increases (Figs. 13(a) and 13(b)). No significant reduction in C_D or $C_{D,jet}$ is noticed (Figs. 13(a) and 13(b)). In these cases, the averaged flow pattern is symmetric in the vertical direction (Fig. 12(a)). However, for IR>1, the lift fluctuation is slightly reduced, and significant reductions in C_D or $C_{D,jet}$ are noticeable (Fig. 13(c)). These are related to the change in vortex shedding pattern in this range of IR. Figure 12(b) reveals a symmetry-breaking bifurcation in the flow field, and also shows that the high-pressure region is detached from the front face by the jet, resulting in a considerable drag reduction in both C_D(42.7%) and $C_{D,jet}$ (15.3%). See Table 1.

3.2 Turbulent vortex shedding and scalar transport

An LES is carried out at Re=8 520 for the same

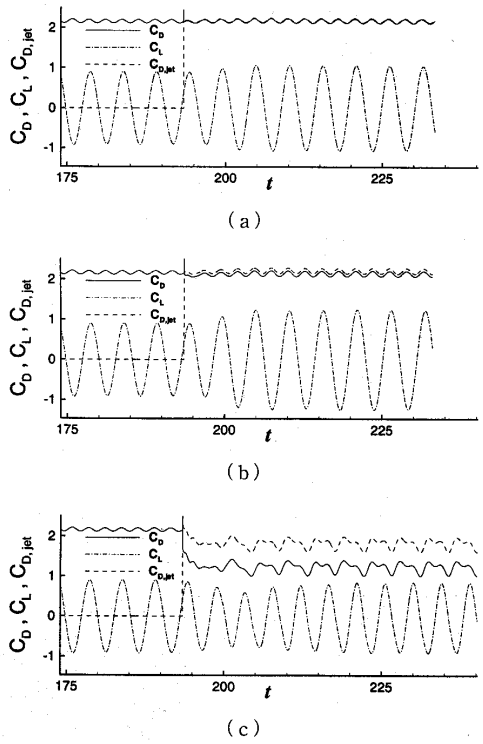

Fig. 13 Drag and lift coefficients for front jet, Re=200; (a) IR=0.235, (b) IR=0.53, (c) IR=1.54. The jet is suddenly injected at t=194.

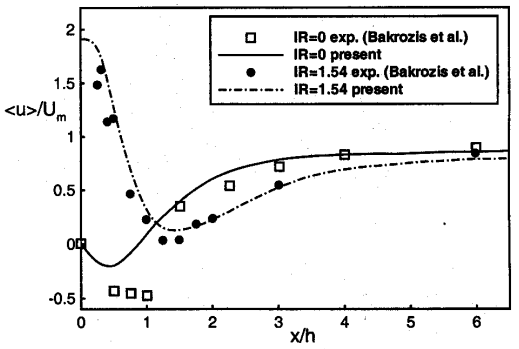

Fig. 14 Distribution of averaged streamwise velocity along the center line, Re=8 520

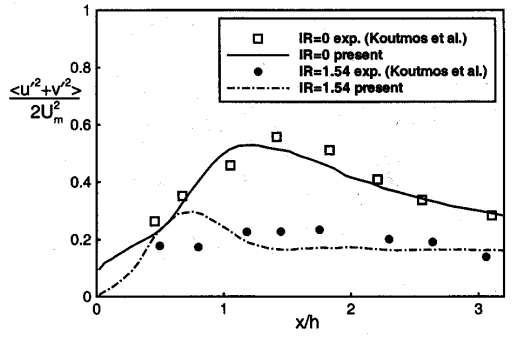

Fig. 15 Distribution of fluctuation energy along the center line, Re=8 520

vertical jet width and blockage ratio as the laminar case in order to study characteristics of turbulent confined vortex shedding and related scalar transport in association with a fuel jet. The spanwise direction is assumed to be homogeneous and a periodic boundary condition is employed in z. A uniform u profile with 0.5% of RMS random fluctuation and ϕ=0 are applied at the inlet as the velocity and ϕ boundary conditions, respectively. At the exit boundary, a convective boundary condition[13] is imposed for both u_i and ϕ. On the solid boundaries, a wall-layer model[16] is used for u_i in order to save a lot of grid points near the wall otherwise required to resolve the near-wall region, and a Neumann condition is imposed for ϕ. A uniform velocity profile and ϕ=1 are prescribed at the jet.

The same values of IR correponding to the laminar cases reported earlier are selected. The spanwise dimension (W) of the computational domain is 1.0h, and a grid system of 192×144×32 is employed after rigorous grid-refinement study.

3.2.1 Averaged fields The centerline distributions of the streamwise velocity and fluctuation energy averaged in time and in z are shown in Figs. 14 and 15, respectively, together with those of the experimental measurements by Koutmos et al.[9] and Bakrozis et al.[17] The averaging is denoted by $\langle\ \rangle$. Considering the high Re and a relatively coarse grid system employed in this study, an excellent agreement with the experimental measurements is obtained. For IR=0, one can identify a recirculation region just behind the cylinder (Fig. 14). That is not the case for IR=1.54 because the pattern of vortex shedding has been changed due to the presence of the jet.

Figure 16 shows the averaged streamlines for the three different values of IR. It is interesting to notice that they look very similar to the laminar counterparts in Fig. 4 even though Re is quite different. The role of the jet explained earlier in the case of laminar vortex shedding seems equivalently applied to the turbulent case.

Figures 17 and 18 represent profiles of averaged streamwise velocity and turbulence intensity at selected streamwise locations; only upper half of the domain is shown because of vertical symmetry. At a location near the cylinder (x/h=0.5), $\langle u\rangle$ in the low-IR cases exhibits wake-type profiles, and $\langle u\rangle$ in the high-IR case shows a jet-type feature in its profile

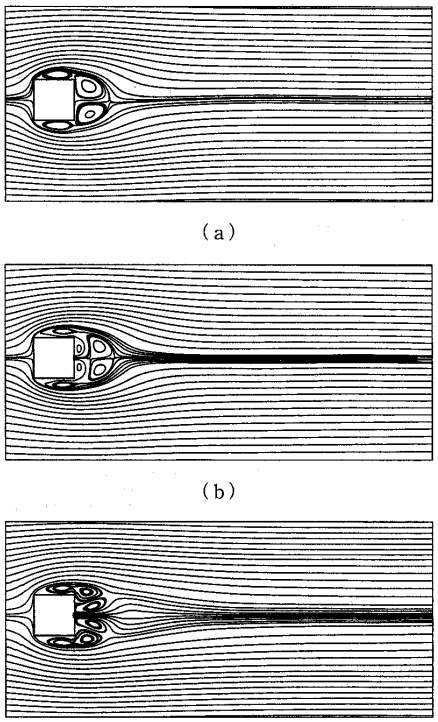

(a) (b) (c)

Fig. 16 Streamlines for time and space (z) averaged velocity fields, Re=8 520; (a) IR=0, (b) IR=0.53, (c) IR=1.54

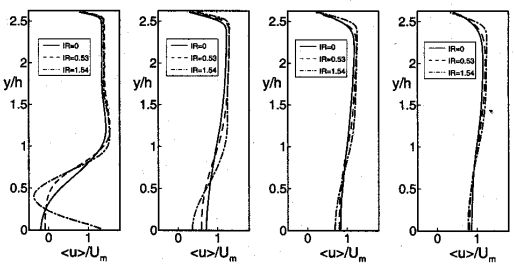

(a) (b) (c) (d)

Fig. 17 Profiles of streamwise mean velocity; (a) x/h =0.5, (b) x/h=2.5, (c) x/h=4.5, (d) x/h=6.5

(Fig. 17). The effect of the jet on $\langle u \rangle$ gradually attenuates downstream of the cylinder; at x/h=4.5 and further downstream, the difference in the profiles seems to be minimal. Turbulence intensity, however, is more significantly influenced by the jet; the difference in the profiles of turbulence intensity is persistent even far downstream of the cylinder (Fig. 18(d)).

Both mean and RMS fluctuation values of C_D and C_L along with St are listed in Table 2. It should be noted that the fluctuations in C_D and C_L are considerably reduced by the presence of the jet; that is not the case for the mean value of C_D or St.

Table 2 Mean and RMS fluctuation values of C_D and C_L

	$C_{D\,mean}$	$C_{D\,RMS}$	$C_{L\,RMS}$	St
IR=0	2.52	0.238	1.463	0.157
IR=0.53	2.63	0.195	1.107	0.154
IR=1.54	2.46	0.109	0.531	-

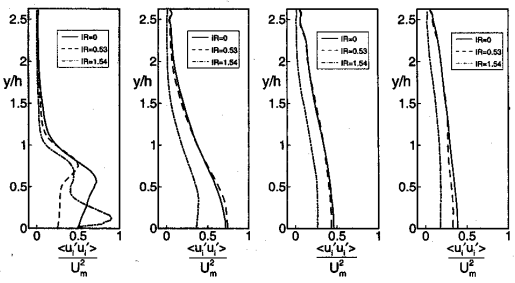

(a) (b) (c) (d)

Fig. 18 Profiles of turbulence intensity; (a) x/h=0.5, (b) x/h=2.5, (c) x/h=4.5, (d) x/h=6.5

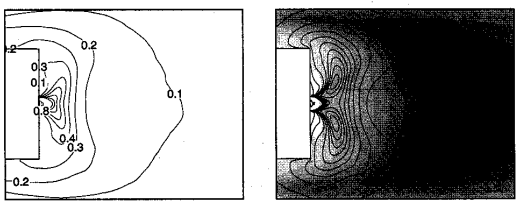

(a) (b)

Fig. 19 Contour plots of time and space (z) averaged scalar fields, Re=8 520, and IR=0.53; (a) mean mass-fraction ($\langle \phi \rangle$; increment, 0.1), (b) scalar fluctuation ($\langle \phi'^2 \rangle$; increment, 0.012); turbulence intensity (gray scale)

Contours of averaged mass fraction ($\langle \phi \rangle$) are shown in Figs. 19(a) and 20(a) for IR=0.53 and 1.54, respectively. Corresponding contours of $\langle \phi'^2 \rangle$ are presented on top of the turbulence intensity distribution in Figs. 19(b) and 20(b), respectively. In the case of IR=0.53 (Fig. 19) in which the jet does not have enough momentum to penetrate the main vortices, the regions of high mass fraction and high scalar fluctuation are formed immediately behind the cylinder; they do not coincide with the region of high turbulence intensity. A strong jet with IR=1.54 (Fig. 20), however, breaks the main vortices; the regions of high mass fraction and high scalar fluctuation are expanded further downstream. Especially, the region of active fuel mixing well coincides with those of high

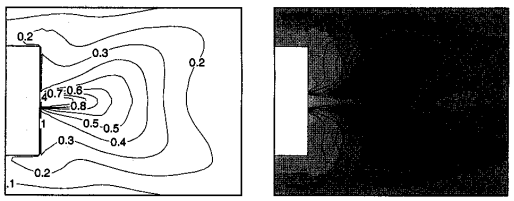

(a) (b)

Fig. 20 Contour plots of time and space (z) averaged scalar fields, Re=8 520 and IR=1.54; (a) mean mass-fraction ($\langle\phi\rangle$; increment, 0.1), (b) scalar fluctuation ($\langle\phi'^2\rangle$; increment, 0.008); turbulence intensity (gray scale)

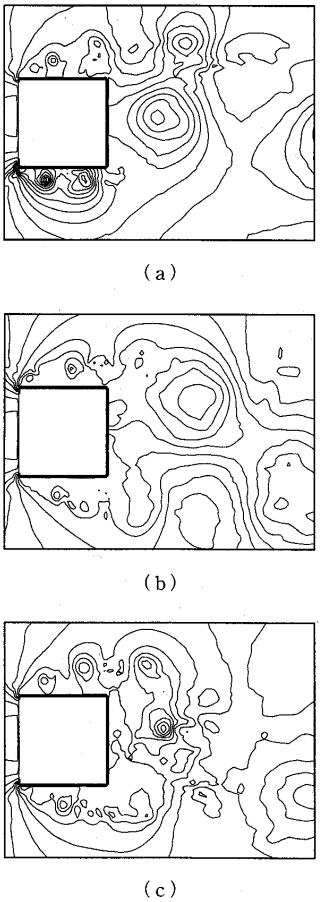

(a)

(b)

(c)

Fig. 21 Contour plots of instantaneous pressure fields $\left(\Delta P \Big/ \frac{1}{2}\rho U_m^2 = 0.4\right)$, Re=8 520; (a) IR=0, (b) IR=0.53, (c) IR=1.54

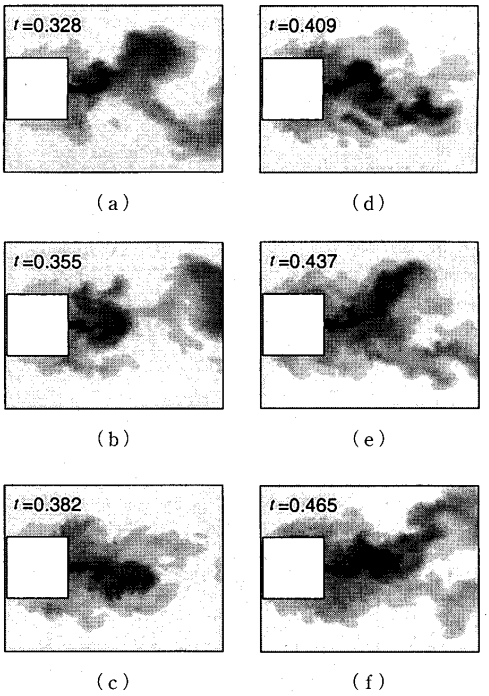

Fig. 22 Sequential contour plots of initial scalar field developed around the bluff-body, Re=8 520, and IR=1.54

turbulence intensity.

3. 2. 2 Instantaneous fields Figure 21 shows instantaneous pressure contours of the flow field near the square cylinder for each IR. It is clearly observed that the vortex is formed at the leading edges, developed and convected downstream. Particularly, for IR=1.54, strong vortices between the jet and the entrained stream are found (Fig. 21(c)).

Figure 22 illustrates the initial stage of scalar transport. The jet is suddenly injected into a developed flow at t=0. Vigorous fuel-air mixing is noticed due to the vortex shedding. Furthermore, a fuel-rich region is sustained near the jet because of the recirculating action of the vortices (Fig. 16(c)); this indicates that the cylinder plays the role as a flame holder to prevent a lean-blow-out. One can also notice that the fuel is being fed upstream through the recirculating region on the top and bottom faces of the cylinder. Figure 23 shows a time-sequence of scalar fields downstream of the cylinder in later stages. Contours of ϕ which acts as a passive scalar clearly visualize vortex shedding, and also shows quick dilution of fuel within a short distance of about 8h from the jet.

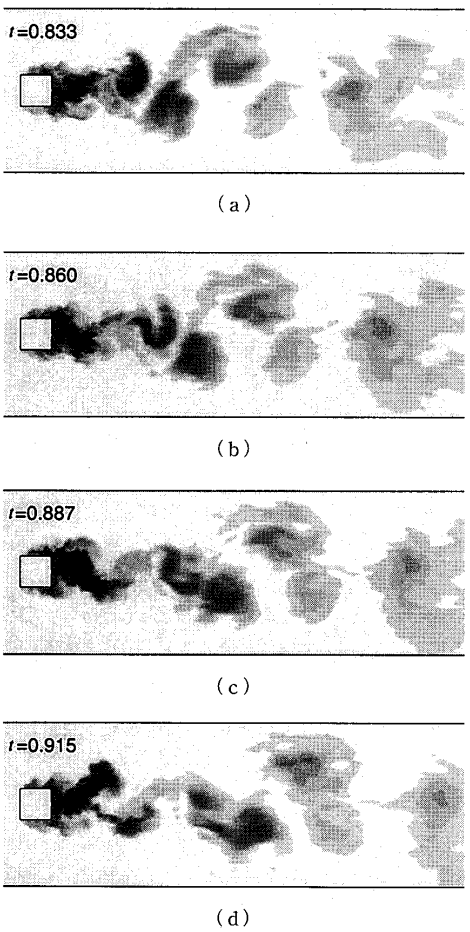

Fig. 23 Sequential contour plots of later scalar field downstream of the cylinder, $Re=8\,520$, and $IR=1.54$

4. Conclusion

Vortex shedding and scalar transport past a square cylinder with a planar jet are numerically studied. The cylinder is located at the middle of two parallel plates; all the flow structures including shed vortices are confined in the channel. The vertical width of the jet is set as $h/8$, and the blockage ratio (H/h) is fixed as 6. Both laminar ($Re=200$) and turbulent ($Re=8\,520$) regimes are considered with various values of IR. If the jet constitutes a flow of fuel, the flow configuration can be regarded as a simple model of a planar combustor where the cylinder plays the role of a flame holder. Depending on IR, the pattern of vortex shedding can change significantly; the force loading on the cylinder can thus be affected accordingly.

For laminar flow, both rear and front jets are considered. Rear jet pushes the main vortices generated by the cylinder further downstream, yielding considerable reduction of fluctuations of C_D and C_L. It turns out that there is an optimum IR for each coefficient which produces minimum fluctuation; $IR=1.2$ for C_D and $IR=1.05$ for C_L. A strong jet ($IR>1.1$) penetrates and breaks the main vortices downstream of the cylinder, resulting in complete disappearance of the main vortices. Simulations of passive scalar show that convection is the dominant mechanism in scalar transport. In case of front jet, the high-pressure region on the front face of the cylinder is pushed upstream by the jet. As a result, drag force exerted on the cylinder can be significantly reduced. A symmetry-breaking bifurcation is also observed for high IR.

LES with a dynamic procedure to determine the model coefficient is employed for turbulent flow with a rear jet. The LES results show a good agreement with the experimental data currently available. The averaged flow fields reveal that the flow structures can be significantly affected by the jet. The pattern of flow-structural change surprisingly resembles that of laminar flow. In contrast to mean velocities, fluctuations are more sensitive to IR downstream of the cylinder. In the case of low IR, the regions of high mass fraction and high scalar fluctuation are identified immediately behind the cylinder; they do not coincide with the region of high turbulence intensity. In the case of a strong jet, however, the regions of high mass fraction and high scalar fluctuation are expanded further downstream; the regions of active scalar mixing well coincide with those of high turbulence intensity. One can notice high mass fraction in the recirculation regions on the upper and lower faces of the cylinder which explains the role of square cylinder in a planar combustor as a flame holder.

5. Acknowlegments

This work was supported by grant No. R01-2002-000-00060-0 from the Basic Research Program of the Korea Science & Engineering Foundation.

References

(1) Kwon, K. and Choi, H., Control of Laminar Vortex Shedding behind a Circular Cylinder Using Splitter Plates, Phys. Fluids, Vol. 8, No. 2 (1995), pp. 479-486.

(2) Duke, R., Shrader, B. and Mo, J., Effects of a Rear Stagnation Jet on the Wake behind a Cylinder, AIAA J., Vol. 31, No. 9, Technical Notes, (1993), pp. 1727-1729.

(3) Park, D.S., Ladd, D.M. and Hendricks, E.W., Feedback Control of von Karman Vortex Shed-

ding behind a Circular Cylinder at Low Reynolds Numbers, Phys. Fluids, Vol. 6, No. 7 (1994), pp. 2390-2405.
(4) Mittal, R., Progress on LES of Flow Past a Circular Cylinder, Annual Research Briefs, (1996), Center for Turbulence Research, Stanford University, Stanford, CA, U.S.A.
(5) Okajima, A., Strouhal Numbers of Rectangular Cylinders, J. Fluid Mech., Vol. 123 (1982), pp. 379-398.
(6) Bosch, G. and Rodi, W., Simulation of Vortex Shedding Past a Square Cylinder with Different Turbulence Models, International Journal for Numerical Methods in Fluids, Vol. 28, No. 4 (1998), pp. 601-616.
(7) Davis, R.W. and Moore, E.F., A Numerical Study of Vortex Shedding from Rectangles, J. Fluids Mech., Vol. 116 (1982) pp. 475-506.
(8) Nakagawa, S., Nitta, K. and Senda, M., An Experimental Study on Unsteady Turbulent near Wake of Rectangular Cylinder in a Channel Flow, Experiments in Fluids, Vol. 27, No. 3 (1999), pp. 284-294.
(9) Koutmos, P., Mavridis, C. and Papailiou, D., A Study of Turbulent Diffusion Flames Formed by Planar Fuel Injection into the Wake Formation Region of a Slender Square Cylinder, Twenty-Sixth Symposium (International) on Combustion/ The Combustion Institute, (1996), pp. 161-168.
(10) Yang, K.S. and Ferziger, J.H., Large-eddy Simulation of Turbulent Obstacle Flow Using a Dynamic Subgrid-scale Model, AIAA Journal, Vol. 31, No. 8 (1993), pp. 1406-1413.
(11) Akselvoll, K. and Moin, P., Large Eddy Simulation of Turbulent Confined Coannular Jets, J. Fluids Mech., Vol. 315 (1996), pp. 387-411.
(12) Kim, J. and Moin, P., Application of a Fractional-Step Method to Incompressible Navier-Stokes Equations, Journal of Computational Physics, Vol. 59, No. 2 (1985), pp. 308-323.
(13) Pauley, L.L., Moin, P. and Reynolds, W.C., A Numerical Study of Unsteady Laminar Boundary Layer Separation, Report No. TF-34, Thermosciences Division, Department of Mechanical Engineering, Stanford University, Stanford, (1988), CA 94305, U.S.A.
(14) Davis, R.W., Moore, E.F. and Purtell, L.P., A Numerical-experimental Study of Confined Flow around Rectangular Cylinder, Phys. Fluids, Vol. 27, No. 1 (1984), pp. 46-59.
(15) Cho, S.H. and Kang, S.H., Simulation of Vortex Shedding from a Square Cylinder in Oscillating Channel Flow, KSME International Journal, Vol. 11, No. 2 (1997), pp. 195-207.
(16) Ciofalo, M. and Collins, M., k-ε Predictions of Heat Transfer in Turbulent Recirculating Flows Using an Improved Wall Treatment, Numerical Heat Transfer, Part B, Vol. 15 (1989), pp. 21-47.
(17) Bakrozis, A.G., Papailiou, D.D. and Koutmos, P., A Study of the Turbulent Structure of a Two-dimensional Diffusion Flame Formed behind a Slender Bluff-body, Combustion and Flame, Vol. 119 (1999), pp. 291-306.